Research Article *Science, Engineering and Health Studies 2020, 14(1), 32-46*

New [5]helicene derivatives with large Stokes shifts for Hg^{2+} determination and their application in drinking water, river water and tuna fillet

Anuwut Petdum[1], Jitnapa Sirirak[1], Vannajan Sanghiran Lee[2], Hubert A. Nienaber[3], Waraporn Panchan[4], Thanasat Sooksimuang[4] and Nantanit Wanichacheva[1*]

[1]*Department of Chemistry, Faculty of Science, Silpakorn University, Nakhon Pathom 73000, Thailand*
[2]*Department of Chemistry, Centre for Theoretical and Computational Physics, Faculty of Science, University of Malaya, Kuala Lumpur 50603, Malaysia*
[3]*Strem Chemicals Inc., Newburyport MA 01950, USA*
[4]*National Metal and Materials Technology Center (MTEC), Pathumthani 12120, Thailand*
[*]*Corresponding author: wanichacheva_n@su.ac.th*

Received: June 26, 2019; Revised: November 12, 2019; Accepted: November 14, 2019

ABSTRACT

Two novel [5]helicene-based fluorescence sensors, **H1** (2,2'-((propane-1,3-diylbis(sulfanediyl))bis(ethane-2,1-diyl))bis(7,12-dimethoxy-4,5,14,15-tetrahydro-1H-dinaphtho[2,1-e:1',2'-g]isoindole-1,3(2H)-dione) and **H1A** (2,2'-((propane-1,3-diylbis(sulfanediyl))bis(ethane-2,1-diyl))bis(7,12-dimethoxy-1H-dinaphtho[2,1-e:1',2'g]isoindole-1,3(2H)-dione) were successfully prepared and characterized for their application in the determination of Hg^{2+} ions. The syntheses of **H1** and **H1A** involved simple reactions including alkylation and imide formation. The spectroscopic results of **H1** and **H1A** showed strong fluorescence in the visible region and large Stokes shifts (150-200 nm). Sensors provided Hg^{2+}-selective fluorescence quenching by discriminating interfering ions including Cd^{2+}, Co^{2+}, Zn^{2+} Pb^{2+}, Ag^{+} and Cu^{2+}. The binding mode of the sensors was also explored using molecular modeling, In addition, **H1** showed the potential to determine Hg^{2+} in real samples such as drinking water, river water and tuna fillet.

Keywords: mercury ion; fluorescence sensor; selectivity; [5]helicene

1. INTRODUCTION

Mercury, a hazardous metal, is toxic to organisms (Renzoni et al., 1998; Harris et al., 2003). Inorganic mercury (Hg^{2+}) can dissolve in water and easily contaminate in the environment. In aquatic ecosystems, microorganisms can change inorganic mercury to organic mercury (CH_3Hg^{+}), which can contaminate marine animals, then accumulate in the human body though oral ingestion (Hardy and Jones, 1997). Mercury can cause many serious human health problems including nerve and DNA damage, leading to Minamata disease. (Gutknecht, 1981; Harada et al., 1995; Tchounwou et al., 2003). Among the techniques for the analysis of Hg^{2+}, fluorescence spectroscopy has been frequently used; it has also been applied to the detection of several agents such as small molecules (Ooyama et al., 2011), protons (H^{+}) (Thivierge et al., 2011), anions (Buckland et al., 2011) and cations (Wanichacheva et al., 2013). Sensors with fluorescent behavior have advantages in terms of low cost, high selectivity, high sensitivity, making the technique suitable for on-site detection (Cheng et al., 2011; Kraithong et al., 2016).

Recently, there have been many Hg^{2+}-fluorescence sensors containing nitrogen and sulfur-

containing crown ionophores such as calixarenes (Lee et al., 2010; Miao et al., 2012; Erdemir et al., 2013), diazatetrathia crown ethers (Kim et al., 2006) and cyclams (Song et al., 1996; Kim et al., 2006; Park et al., 2007). Although these ionophores provide the crown structure, they have limitations such as the high cost of commercial compounds, the multi-step syntheses and low selective detection or cross sensitivity to other metal ions such as Pb^{2+}, Ag^{+}, and Cu^{2+} (Moon et al., 2004; Suresh et al., 2010; Dalapati et al., 2011). Moreover, some previously reported Hg^{2+}-fluorescence sensors consisted of fluorescence dyes with emissions in the UV region and small Stokes shifts, which can cause problems in the analytical process including matrix interference and analytical error.

In this work, the sensors, **H1** and **H1A**, consisted of 2-(3-(2-*aminoethylsulfanyl*) propylsulfanyl) ethanamine (thioether ionophore) and [5]helicene derivatives were designed and synthesized to serve as Hg^{2+} fluorescence sensors (Figure 1). The thioether ionophore, containing nitrogen and sulfur atoms, was employed as the selective ionophore for Hg^{2+}, while, for fluorophore, the [5]helicene derivatives were chosen due to their excellent fluorescence response in the visible region, high quantum yield (~0.9), and large Stokes shift, which could avoid matrix interference and prevent self-absorption (Sooksimuang and Mandal, 2003; Sahasithiwat et al., 2010). Hg^{2+} sensing of **H1** and **H1A** was also studied and their applications in real samples including drinking water, river water and seafood were investigated.

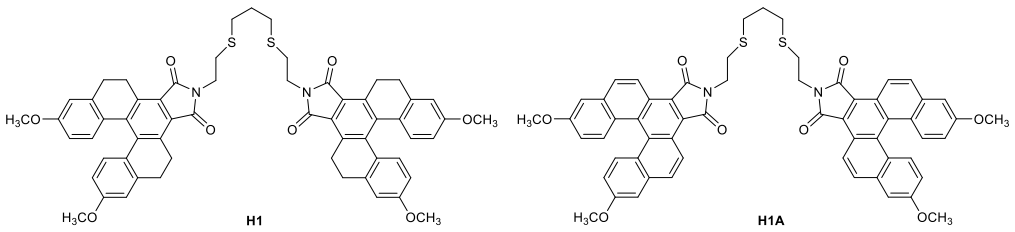

Figure 1 Chemical structure of **H1** and **H1A**

2. MATERAILS AND METHODS

2.1 Materials

All reagents and solvents were purchased from Fluka Chemical Corporation and were used without further purification. Perchlorate salts of metal ions for ion-sensing studies were purchased form Strem Chemicals, Inc. The cation-sensing tests were conducted in acetonitrile solutions. Stock solutions of perchlorate salts (1.0×10^{-2} M) were prepared in acetonitrile.

2.2 Characterization

All compounds were characterized by nuclear magnetic resonance (NMR) spectrometry and mass spectrometry. NMR spectra were obtained in deuterochloroform ($CDCl_3$) with either a Bruker Avance 300 spectrometer operating at 300 MHz for ^{1}H and 75 MHz for ^{13}C or a Bruker AV500 Biospin spectrometer operating at 500 MHz for ^{1}H and 125 MHz for ^{13}C, with TMS as the internal standard. Mass spectra were obtained by a Thermo Electron LCQ-DECA-XP, electrospray ionization ion trap mass spectrometer. Melting points were determined using either a Stuart Scientific melting point apparatus SMP2 or a Mel-Temp melting point apparatus-electrothermal. Absorption spectra were recorded using a Hewlett Packard 8453 spectrophotometer. Fluorescence measurements were carried out with a Perkin Elmer Luminescence spectrometer LS 50B. Fluorescence studies were performed in a quartz cuvette (1 cm × 1 cm), with excitation and emission

slid widths of 5.0 nm, and a scan rate of 300 nm/min. The studies were performed in a quartz cuvette (1 cm × 1 cm), with excitation and emission slid widths of 5.0 nm, and a scan rate of 300 nm/min. The fluorescence experiments were carried out by the titration of heavy metal ions with **H1** (4.0×10^{-8} M) and **H1A** (1.1×10^{-6} M). The excitation wavelengths of **H1** and **H1A** were fixed at 373 nm and 335 nm, respectively.

2.3 Syntheses

2.3.1 2-[3-(2-Aminoethylsulfanyl) propylsulfanyl] ethanamine

The synthesis of the title compound was reported in our previous work (Wanichacheva et al., 2009). Briefly, the alkylation of cysteamine hydrochloride with 1,3-dibromopropane in the presence of sodium hydroxide as a base gave the title compound quantitative yield (Figure 2).

*2.3.2 7,12-Dimethoxy-4,5,14,15-tetrahydronaphtho [2',1':3,4]phenanthrol[1,2-c]furan-1,3-dione (**M201**)*

Synthesis of the title compound was reported in our previous work (Sooksimuang et al., 2014). Briefly, the Diels-Alder reaction followed by oxidation of 6,6′-dimethoxy-3,4,3′,4′-tetrahydro[1,10]binaphthalenyl obtained **M201**, 31% in two steps (Figure 3). The maleic anhydride and diene were mixed and stirred in toluene to obtain the adduct from the Diels-Alder reaction. The Diels-Alder adduct was then oxidized using 2,3-dichloro-5,6-dicyano-1,4-benzoquinone (DDQ) as a reagent to yield the title compound as a yellow solid.

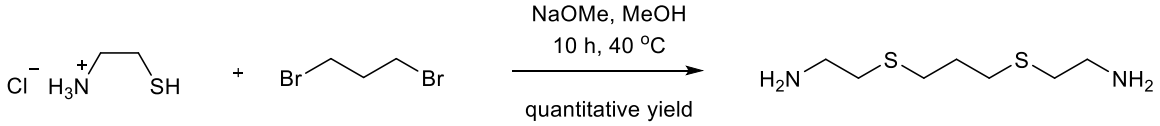

Figure 2 Synthesis of 2-[3-(2-aminoethylsulfanyl) propylsulfanyl] ethanamine

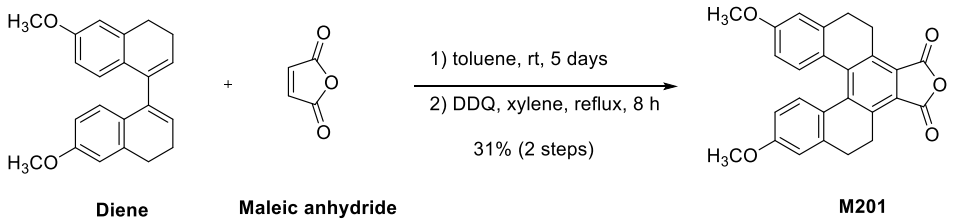

Figure 3 Synthesis of **M201**

*2.3.3 7,12-Dimethoxynaphtho[2',1':3,4] phenanthrol[1,2-c]furan-1,3-dione (**M201A**)*

A mixture of *7,12-dimethoxy-4,5,14,15-tetrahydronaphtho[2',1':3,4]phenanthro[1,2-c]furan-1,3-dione*, **M201**, (1.45 g, 3.52 mmol), benzoyl peroxide (0.11 g, 0.34 mmol), and *N*-bromosuccinimide (NBS) (1.38 g, 7.74 mmol) was dissolved in benzene (90 mL) and the mixture was refluxed for 7 h. A solution of sodium acetate (NaOAc) (1.91 g, 23.23 mmol) in acetic acid (AcOH) (30 mL) was then added to the solution mixture and it was refluxed for an additional 15 h. The solution mixture was then cooled down to room temperature and washed with deionized water (150 mL). The organic portion was collected and dried over anhydrous sodium sulfate (anh. Na_2SO_4). The solvent was then removed under vacuum to yield a

crude product. Crystallization from chloroform gave the pure product, **M201A** (Figure 4) as orange needles (1.02 g, 71%), mp. 317-318°C. Fourier-transform infrared (FT-IR) ((potassium bromide (KBr)): 3008, 2942, 2840, 1827, 1762, 1609, 1523, 1499, 1462, 1435, 1349, 1272, 1241, 1193, 1181, 1168, 1153, 1124, 1065, 1021, 906, 854, 825, 811, 735, 695 cm^{-1}. 1H NMR (300 MHz, $CDCl_3$) δ (ppm): 3.99 (s, 6H), 6.92 (dd, *J* = 9.3, 2.7 Hz, 2H), 7.29 (d, *J* = 2.7 Hz, 2H), 8.02 (d, *J* = 8.7 Hz, 2H), 8.24 (d, *J* = 9.3 Hz, 2H), 8.83 (d, *J* = 8.9 Hz, 2H). 13C NMR (75 MHz, CDCl3) δ (ppm): 55.5 ($2CH_3$), 107.4 (2CH), 116.9 (2CH), 121.7 (2CH), 125.2 (2C), 125.4 (2C), 125.7 (2C), 130.2 (2CH), 130.9 (2CH), 132.6 (2C), 135.7 (2C), 159.8 (2C), 163.7 (2C=O). High-resolution mass spectrometry (HRMS): micro time-of-flight (microTOF) calculated for $C_{26}H_{16}O_5H^+$ 409.1076 m/z, found 409.1076 m/z.

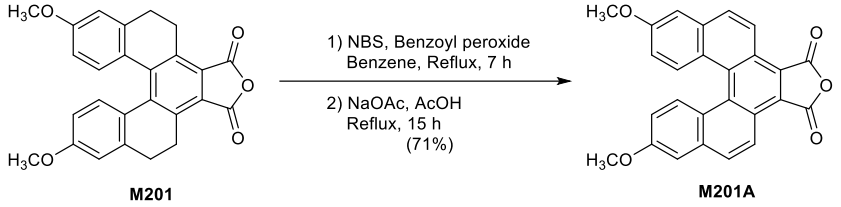

M201 M201A

Figure 4 Synthesis of **M201A**

*2.3.4 Sensor **H1***

In a round bottom flask, a mixture of 2-[3-(2-aminoethylsulfanyl)propylsulfanyl]ethanamine (0.05 g, 0.26 mmol), potassium carbonate (K_2CO_3) (0.15 g, 1.1 mmol) and 7,12-dimethoxy-4,5,14,15-tetrahydronaphtho[2',1':3,4]phenanthro[1,2-c]furan-1,3-dione (**M201**) (0.22 g, 0.54 mmol) was stirred and heated to 110°C in dimethylformamide (DMF) (3.5 mL) for 3 h under an argon atmosphere. The reaction mixture was then cooled down to room temperature; deionized water (20 mL) was added and the mixture was stirred for 1 h. The mixture was then filtered to give a yellow solid which was purified by preparative thin layer chromatography using ethyl acetate: hexane = 1:2 (R_f = 0.56) to yield 0.133 g of a yellow solid, 52%.mp = 158.0-161.4°C, ^{1}H NMR ($CDCl_3$, 300 MHz) δ (ppm): 1.91 (p, *J* = 6.9 Hz, 2H), 2.47 (broad, 4H), 2.73 (t, *J* = 6.9 Hz, 4H), 2.75-2.84 (m, 12H), 3.81 (s, 12H), 3.86 (broad, 4H), 4.09 (m, 4H), 6.48 (d, *J* = 2.1 Hz, 2H), 6.51 (d, *J* = 2.4 Hz, 2H), 6.80 (s, 2H), 6.81 (s, 2H), 7.13 (d, *J* = 4.8 Hz, 2H), 7.16 (d, *J* = 4.5 Hz, 2H). ^{13}C NMR ($CDCl_3$, 75 MHz,) δ (ppm): 24.2 ($4CH_2$), 28.9 ($4CH_2$), 29.0 (CH_2), 29.9 ($2CH_2$), 30.4 ($2CH_2$), 36.8 ($2CH_2$), 55.2 ($4CH_3$), 111.8 (4CH), 112.5 (4CH), 125.1 (4C), 126.5 (8C), 131.3 (4CH), 138.0 (4C), 141.0 (4C), 159.4 (4C), 168.8 (4C=O). HRMS (ESI) calculated for $C_{59}H_{54}N_2O_8S_2Na^+$ $(M+Na)^+$ 1005.3219 m/z, found 1005.3200 m/z.

*2.3.5 Sensor **H1A***

A mixture of 2-[3-(2-aminoethylsulfanyl) propylsulfanyl]ethanamine (0.012 g, 0.062 mmol), 7,12-dimethoxynaphtho[2',1':3,4]phenanthrol[1,2-c]furan-1,3-dione (**M201A**) (0.056 g, 0.14 mmol) and K_2CO_3 (0.025 g, 0.18 mmol) in dimethylformamide (2.0 mL) was stirred and heated to 80ºC for 1 h under an argon atmosphere. The mixture was cooled down to room temperature followed by solvent removal under vacuum. Dichloromethane (20 mL) was added and the mixture was washed with deionized water (3 × 20 mL). The crude product was purified by column chromatography using 0.5% triethylamine in ethyl acetate: hexane (1:2) to give 0.023 g of an orange solid (Figure 5), 38%. mp = 157.0-159.7°C, ^{1}H NMR ($CDCl_3$, 300 MHz) δ (ppm): 2.17 (p, 2H), 2.80-3.95 (m, 8H), 3.83-3.98 (s, 16H), 6.58 (dd, 4H), 7.05 (d, 4H), 7.70 (d, 4H), 7.78 (d, 4H), 8.75 (d, 4H). ^{13}C

NMR ($CDCl_3$, 75 MHz,) δ (ppm): 28.6 (CH_2), 29.01 ($2CH_2$), 29.67 ($2CH_2$), 37.0 ($2CH_2$), 55.4 ($4CH_3$), 107.1 (4CH), 115.7 (4C+4CH), 121.6 (4CH), 125.0 (4C), 128.9 (4C+4CH), 130.5 (4C+4CH), 134.6 (4C), 158.7 (4C), 169.3 (4C=O); HR-ESI MS calculated for $C_{33}H_{32}N_2O_4S_2K^+$ $(M+K)^+$ 1013.2333 m/z, found 1013.2419 m/z.

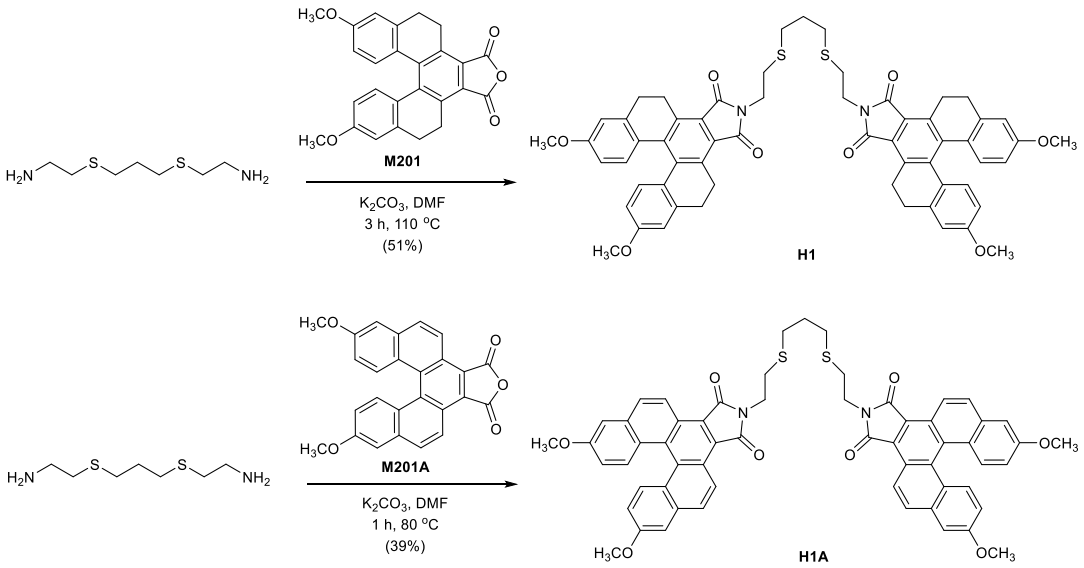

Figure 5 Synthesis of **H1** and **H1A**

2.4 Computational methods

Density functional theory calculations at the Becke's 3-Parameter with Lee, Yang and Parr (B3LYP) density functional with 6-311G** for main group element and LanL2DZ for Hg^{2+} were carried out using the Gaussian 09 program (Frisch et al., 2016; Shellaiah et al., 2015). The solvation by acetonitrile was modeled by the integral equation formalism polarizable continuum model (IEEPCM). Molecular orbital analysis was performed with Gaussian09 and MO pictures were generated using the visual molecular dynamics (Humphrey et al., 1996).

3. RESULTS AND DISCUSSION

3.1 The design of H1 and H1A

Due to the requirements of the highly sensitive and selective Hg^{2+} fluorescence sensors, fluorophores (**M201** and **M201A**) with strong fluorescence quantum yields and thioether ionophore containing nitrogen and sulfur atoms for strong electrostatic interaction to Hg^{2+} were selected. **M201** and **M201A** are derivatives of [5]helicene which possess two methoxy groups as the electron-donating groups and the anhydride group as an electron-withdrawing group (Figure 6). The positions of withdrawing groups (carboxyl group) and electron donating (methoxy group) were placed into an Λ-shape, resulting in an effective push-pull system and strong fluorescence quantum yields.

Sensor **H1** consisted of two units of **M201** while sensor **H1A** contained two units of **M201A**, but with a fully conjugated structure. We anticipated that the high sensitivity of the sensors could be induced by the high fluorescence quantum yields of these fluorophores. The selective binding of the sensors could also take place by ion-dipole interaction between Hg^{2+} and nitrogen and sulfur atoms of the ionophore.

Herein, thioether ionophore (Wanichacheva et al., 2009) was synthesized by alkylation of 1,3-

dibromopropane with cysteamine hydrochloride under basic conditions to give the ionophore in quantitative yield. The fluorophore portion, **M201** (Sooksimuang et al., 2014), was obtained by a Diels-Alder reaction followed by oxidation. **M201A** was obtained by aromatization of **M201** by bromination followed by hydrobromic acid elimination. Sensors **H1** and **H1A** were obtained by imide formation of **M201** and **M201A** with thioether ionophore, respectively.

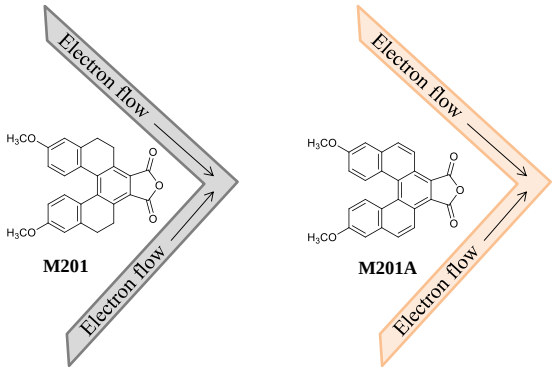

Figure 6 Electron flow from the methoxy groups to the anhydride groups on the Λ-shape structures of **M201** and **M201A**

3.2 Spectroscopic studies

As can be seen in Figure 7, the spectroscopic studies of the sensors conducted in acetonitrile solutions showed that the absorption spectra of **H1** and **H1A** exhibited maximum spectra at 373 and 335 nm, respectively. Moreover, the fluorescence emission spectra of **H1** and **H1A** appeared at 523 and 533 nm, respectively, indicating very large Stokes shifts of 150 and 198 nm, respectively. The wide Stokes shifts of the sensors could be beneficial for the removal of interference from self-absorption (Goswami et al., 2014; Gu et al., 2015).

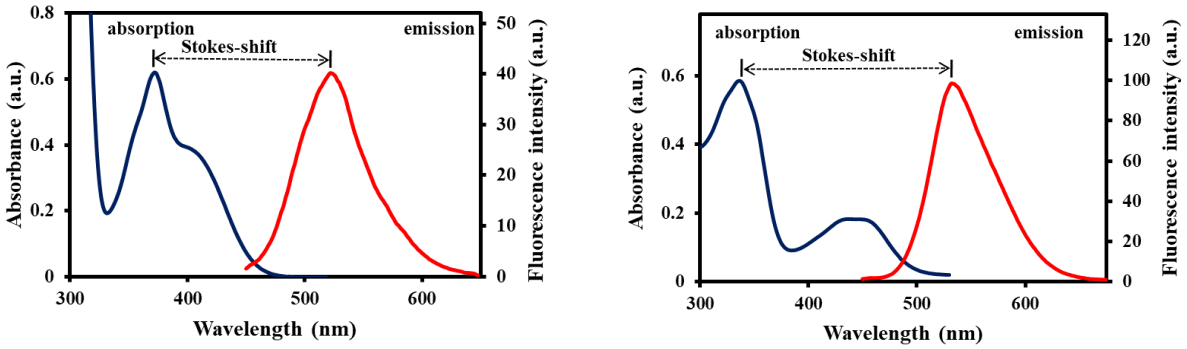

Figure 7 Absorption spectra (0.03 mM) and emission spectra of a **H1** (0.04 μM) and b **H1A** (1.0 μM)

3.3 Sensitivity studies

Hg^{2+} was added into the **H1** and **H1A** solutions and their emission responses were observed to explore the sensitivity of the sensors. Figure 8 and 9 demonstrate that **H1** and **H1A** exhibited high Hg^{2+}-sensitivity from the emission of the modified [5]helicene derivatives centered at about 523 and 533 nm, respectively. In the absence of Hg^{2+}, the sensors

provided strong fluorescence signals. In contrast, the fluorescence quenching of sensors occurred when Hg^{2+} was coordinated with the sensors. The fluorescence quantum yield (Φ_f) of **H1** and **H1A** were 0.92 (using 9,10-diphenylanthracene standard) and 0.032 (using anthracene standard), respectively, while Φ_f of **H1-**Hg^{2+} and **H1A-**Hg^{2+} were 0.17 and 0.016, respectively. Herein, **H1** was found to be a superior sensor to **H1A** in terms of quantum efficiency and sensitivity. In addition, this observation indicated the operation of photoinduced electron transfer process.

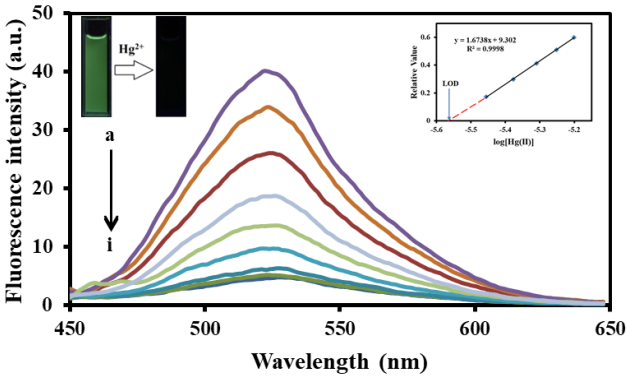

Figure 8 Fluorescence spectra (λ_{ex} 373 nm) of **H1** (0.04 µM) in acetonitrile as a function of increasing [Hg^{2+}]. a: 0 µM, b: 3.5 µM, c: 4.9 µM, d: 6.3 µM, e: 7.7 µM, f: 10.2 µM, g: 17.2 µM, h: 24.2 µM and i: 31.2 µM

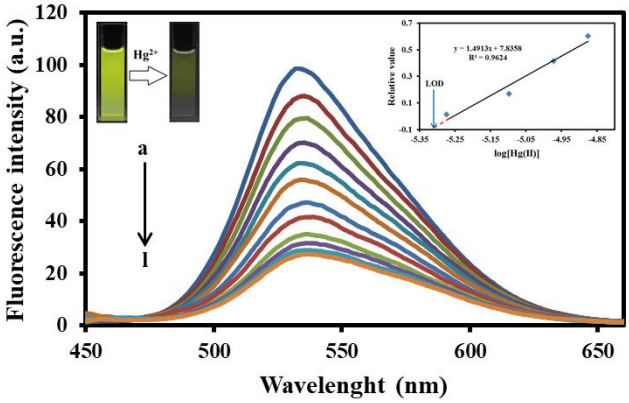

Figure 9 Fluorescence spectra (λ_{ex} 335 nm) of **H1A** (1.0 µM) in acetonitrile as function of increasing [Hg^{2+}]. a: 0 µM, b: 8.0 µM, c: 9.3 µM, d: 10.7 µM, e: 12.0 µM, f: 13.3 µM, g: 16.0 µM, h: 18.7 µM, i: 25.3 µM. j: 32.0 µM, k: 45.3 µM and l: 58.7 µM

Job's experiments were conducted to explore the stoichiometry of the **H1:**Hg^{2+} and **H1A**:Hg^{2+}. According to the results revealed in Figure 10, the possible stoichiometric of **H1:**Hg^{2+} and **H1A**:Hg^{2+} were 1:2 and 1:1, respectively. The association constant was also calculated using a Benesi-Hildebrand equation (Tian et al., 2010; Li et al., 2012) and found to be 2.75×10^{11} M^{-2} with 1:2 of **H1**:2Hg^{2+} and 8.17×10^{5} M^{-1} with 1:1 of **H1A**:Hg^{2+}, which was agreed with the results from Job's experiments. Additionally, the detection limits of **H1** and **H1A** calculated by the plot of fluorescence intensity versus the Hg^{2+} concentrations were 2.8×10^{-6} M and 5.6×10^{-6} M for Hg^{2+} ions, respectively (Shortreed et al., 1996). It should be noted that, **H1** was found to be a

superior sensor to **H1A**, not only in terms of quantum efficiency and sensitivity, but also in terms of the lower detection limit for detection of Hg^{2+}.

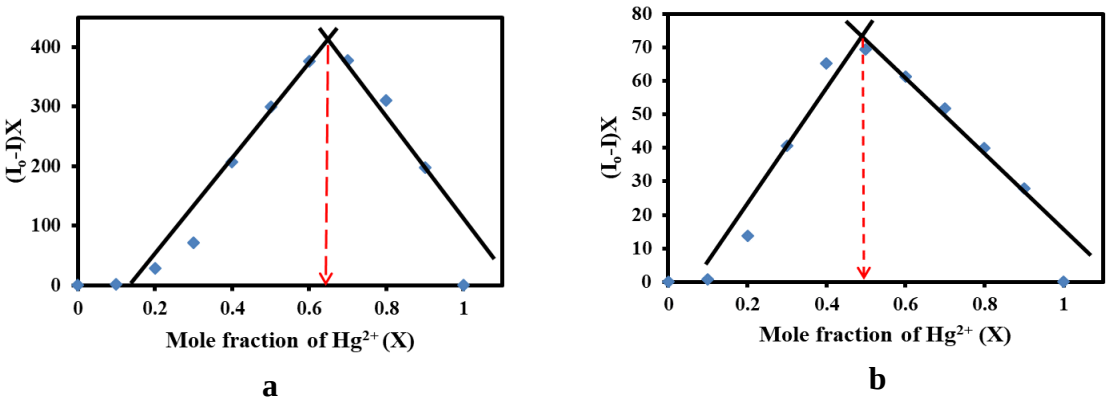

Figure 10 Job's plots for (a) **H1** with Hg^{2+} and (b) **H1A** with Hg^{2+}

3.4 Selectivity studies

By comparison, for the fluorescence signals of a series of separate solutions where each solution contained only a salt of the desired ions including Hg^{2+}, Cu^{2+}, Co^{2+}, Ag^{+}, Ba^{2+}, Pb^{2+}, Ca^{2+}, Fe^{2+}, Cd^{2+}, Na^{+}, K^{+}, Li^{+}, Mg^{2+} and Zn^{2+}, the selectivity studies of **H1** and **H1A** were explored and the results were represented in Figure 11 and Figure 12. It was found that only Hg^{2+} caused fluorescence quenching of sensors, indicating the Hg^{2+}-selectivity of the sensors.

The Hg^{2+}-selective binding of sensors **H1** and **H1A** were noticeable from the images under UV- light**.** The explicit color changes were clearly observed. When Hg^{2+} was added to a solution of **H1**, the color of the solution was changed from fluorescent green to colorless (Figure 13). In addition, the color of the **H1A** solution was changed from yellowish green to light brown when Hg^{2+} was added (Figure 14). In contrast, the colors of the **H1** and **H1A** solutions remained unchanged in the presence of interfering metal ions such as Cu^{2+}, Co^{2+}, Ag^{+}, Ba^{2+}, Pb^{2+}, Ca^{2+}, Fe^{2+}, Cd^{2+}, Na^{+}, K^{+}, Li^{+}, Mg^{2+} and Zn^{2+}.

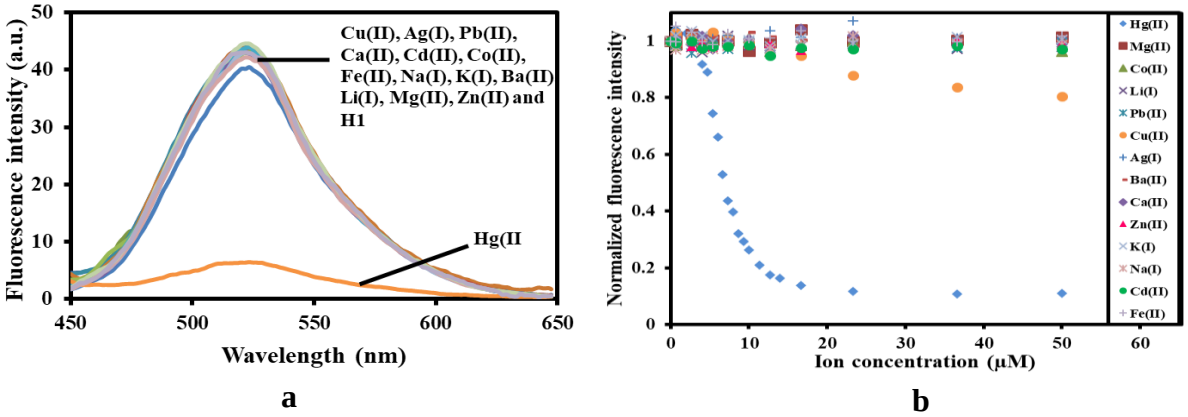

Figure 11 (a) Fluorescence spectra of **H1** (0.04 μM) with perchlorate salts of Hg^{2+}, Cu^{2+}, Co^{2+}, Ag^{+}, Ba^{2+}, Pb^{2+}, Ca^{2+}, Fe^{2+}, Cd^{2+}, Na^{+}, K^{+}, Li^{+}, Mg^{2+} and Zn^{2+}(16.7 μM) and (b) normalized fluorescence intensity of **H1** (0.04 μM) vs the concentrations of various metal ions

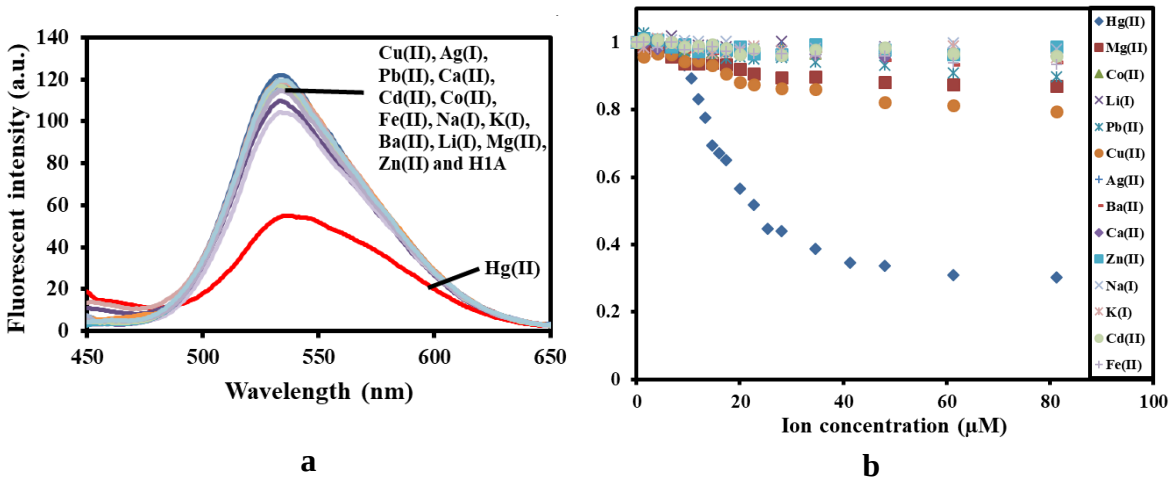

a b

Figure 12 (a) Fluorescence spectra of **H1A** (1.1 μM) with perchlorate salts of Hg^{2+}, Cu^{2+}, Co^{2+}, Ag^{+}, Ba^{2+}, Pb^{2+}, Ca^{2+}, Fe^{2+}, Cd^{2+}, Na^{+}, K^{+}, Li^{+}, Mg^{2+} and Zn^{2+} (34.6 μM) and (b) normalized fluorescence intensity of **H1A** (1.1 μM) in acetonitrile vs the concentrations of various metal ions

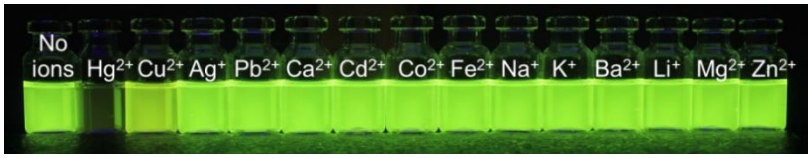

Figure 13 Color changes of **H1** (0.10 μM) in acetonitrile solutions with different metal ions (Hg^{2+}, Cu^{2+}, Co^{2+}, Ag^{+}, Ba^{2+}, Pb^{2+}, Ca^{2+}, Fe^{2+}, Cd^{2+}, Na^{+}, K^{+}, Li^{+}, Mg^{2+} and Zn^{2+} (11 μM)) under UV light

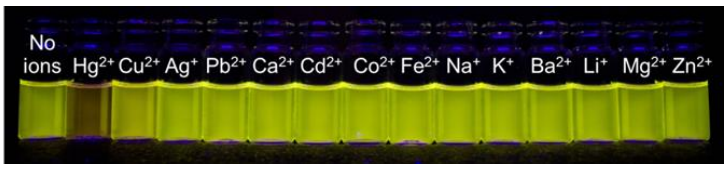

Figure 14 Color changes of **H1A** (12 μM) in acetonitrile solutions with different metal ions (Hg^{2+}, Cu^{2+}, Co^{2+}, Ag^{+}, Ba^{2+}, Pb^{2+}, Ca^{2+}, Fe^{2+}, Cd^{2+}, Na^{+}, K^{+}, Li^{+}, Mg^{2+} and Zn^{2+}(17 μM)) under UV light

Moreover, the competitive studies of the sensors illustrated good selectivity to Hg^{2+}. Figure 15 shows the competitive signaling behaviors of sensors **H1** and **H1A** with Hg^{2+} in the presence of different metal ions (Cu^{2+}, Co^{2+}, Ag^{+}, Ba^{2+}, Pb^{2+}, Ca^{2+}, Fe^{2+}, Cd^{2+}, Na^{+}, K^{+}, Li^{+}, Mg^{2+} and Zn^{2+}) as background. The fluorescence emission provided a relatively consistent Hg^{2+}-induced fluorescence quenching in 10 equivalents of the competing ions. Both sensors, **H1** and **H1A**, gave similar results indicating that the operation of the sensors in determining Hg^{2+} concentrations was not dramatically affected by various metal ions in high concentrations.

3.5 Reversibility studies

Sensors H**1** and **H1A** showed reversible properties with the addition of the reversing reagent. Owing to the high complex formation constant between ethylenediamine (**en**) and Hg^{2+} (5.13×10^{11} M^{-1}) (Bjerrum et al., 1950), **en** was chosen as the reversing

reagent. The **en** could also dissociate the Hg^{2+}-sensor complexes through the ligand exchange process. Figure 16 elucidates that **H1** and **H1A** provided fluorescence quenching after addition of Hg^{2+}; however, the fluorescence quenching disappeared upon addition of **en**. This process could be repeated at least three times, indicating that **H1** and **H1A** had the reversible properties for sensing Hg^{2+} ion.

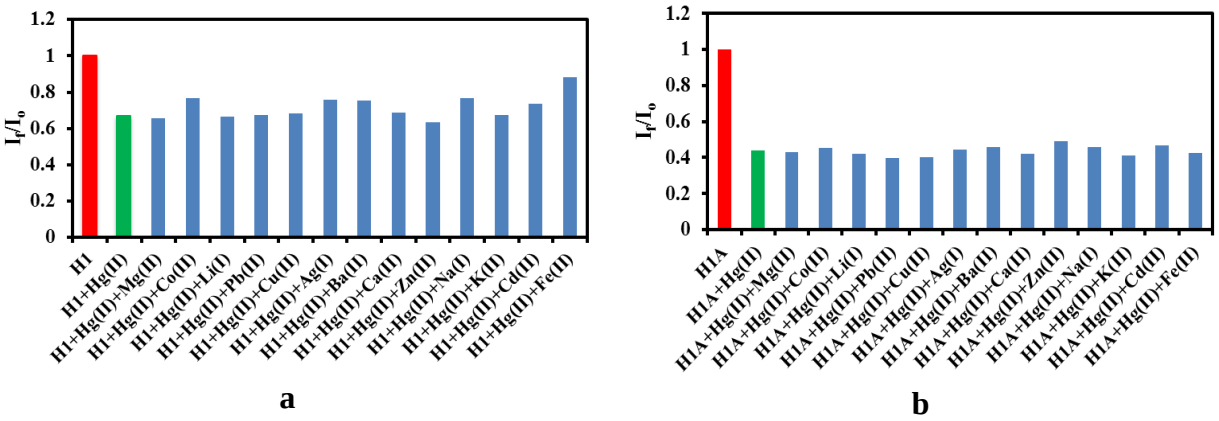

a **b**

Figure 15 (a) Competitive experiments (at 523 nm) in the **H1**-Hg^{2+} system with various metal ions: [**H1**] = 0.04 μM, [Hg^{2+}] = 4.0 μM and [M^{n+}] = 40.0 μM; (b) competitive experiments (at 533 nm) in the **H1A**-Hg^{2+} system with various metal ions: [**H1A**] = 1.1 μM, [Hg^{2+}] = 16.0 μM and [M^{n+}] = 160 μM

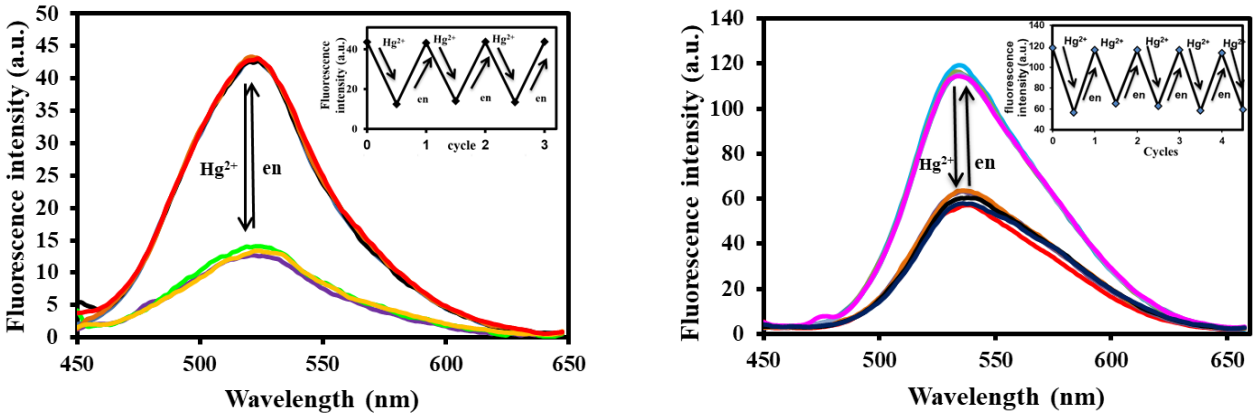

a **b**

Figure 16 Reversibility of sensor-Hg^{2+} systems by ethylenediamine (**en)**: (a) fluorescence spectra of **H1** upon alternating additions of Hg^{2+} and **en**, [**H1**] = 0.04 μM, Hg^{2+} 1 equivalent and **en** 1 equivalent; (b) fluorescence spectra of **H1A** upon alternating additions between Hg^{2+} and en, [**H1A**] = 1.1 μM, Hg^{2+} 1 equivalent and **en** 1 equivalent

3.6 Computational studies

To explore the **H1** and **H1A** structures and the Hg^{2+} bonding to **H1** and **H1A**, molecular modeling was conducted using Gaussian 09 (Frisch et al., 2016) **H1**, **H1A**, **H1**:Hg^{2+} and **H1A**:Hg^{2+}, shown in Figure 17, were obtained at the B3LYP using LanL2DZ (Shellaiah et al., 2015) for Hg^{2+} and 6-311G** for main group element in acetonitrile as solvent with IEFPCM. The initial structures of **H1**:Hg^{2+} and **H1A**:Hg^{2+} were designed based on the results from Job's plot showing

that the ligand:metal ratios for **H1**:Hg^{2+} and **H1A**:Hg^{2+} were 1:2 and 1:1, respectively. Comparison of the optimized structures of **H1** and **H1A** revealed that the two [5]helicene moieties of **H1** were closer to each other than the closeness between the two [5]helicene moieties of **H1A**. The distance between the two centroids No.3 of both [5]helicene moieties in **H1** was 11.13 Å while the corresponding distance was 15.25 Å in **H1A**. For the optimized structures of **H1**:Hg^{2+} and **H1A**:Hg^{2+}, each Hg^{2+} ion in the **H1**:Hg^{2+} was bonded to one oxygen atom and one sulfur atom at distances of 2.85-2.89 Å and 3.36-3.37 Å, respectively whereas the Hg^{2+} in the **H1A**:Hg^{2+} was bonded to two sulfur atoms at distances of 2.88 and 2.94 Å.

These molecular modeling results also indicated that the **H1** sensor (non-fully conjugated fluorophore) was more flexible and provided self-assembly to $2Hg^{2+}$ from the favorable electrostatic interactions of sulfur atoms of the ligands and oxygen atoms of fluorophores to $2Hg^{2+}$ atoms, leading to a likely helical wrapping-like structure. In contrast, the sensor **H1A (**fully conjugated fluorophore) was more rigid compared to **H1** sensor provided the suitable pocket and binding site for one atom of Hg^{2+} by binding to two sulfur atoms and two oxygen atoms at distances of 2.88 and 2.94 Å, as well as binding to two oxygen atoms at distances of 4.98 and 5.38 Å.

HOMO, LUMO and the HOMO-LUMO energy gap of **H1**, **H1A**, **H1**:Hg^{2+} and **H1A**:Hg^{2+} were also examined and shown in Figure 18. The HOMO and LUMO of H**1** and **H1A** were ligand-based π^* orbitals where one [5]helicene moiety dominated the HOMO and another [5]helicene moiety dominated the LUMO. The HOMO-LUMO energy gaps of **H1** and **H1A** were similar at 72.735 and 68.850 kcal/mol, respectively. For the **H1**:Hg^{2+} and **H1A**:Hg^{2+}, their HOMOs were composed principally of π electron clouds on one [5]helicene moiety while significant electron density was found on one Hg^{2+} ion in their LUMO. The HOMO-LUMO energy gaps of the **H1**:Hg^{2+} and **H1A**:Hg^{2+} were 54.367 and 65.782 kcal/mol, respectively.

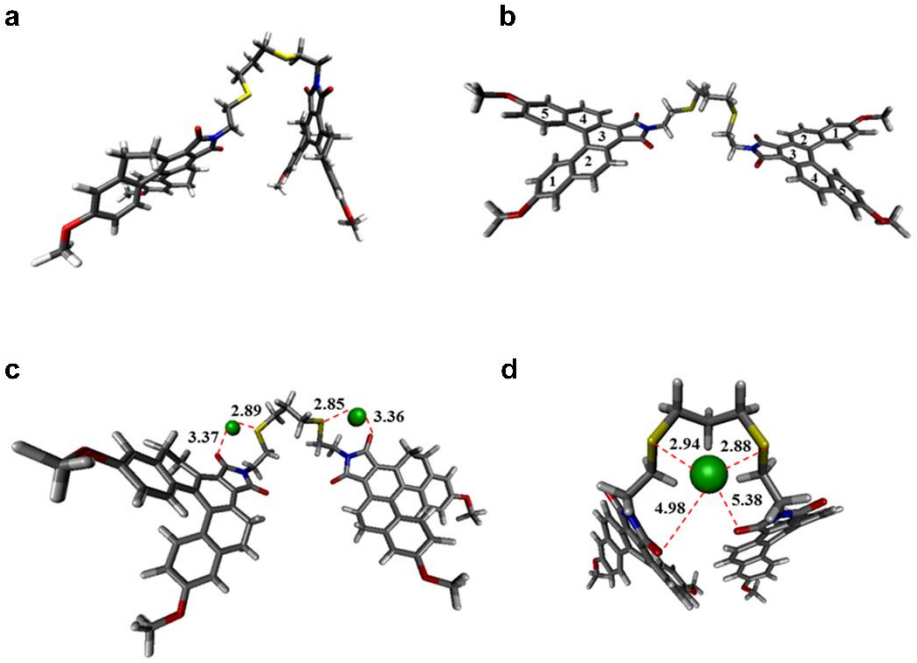

Figure 17 (a) Optimized structure of **H1**; (b) optimized structure of **H1A**; (c) optimized structure of **H1**:Hg^{2+}; (d) optimized structure of **H1A**:Hg^{2+}

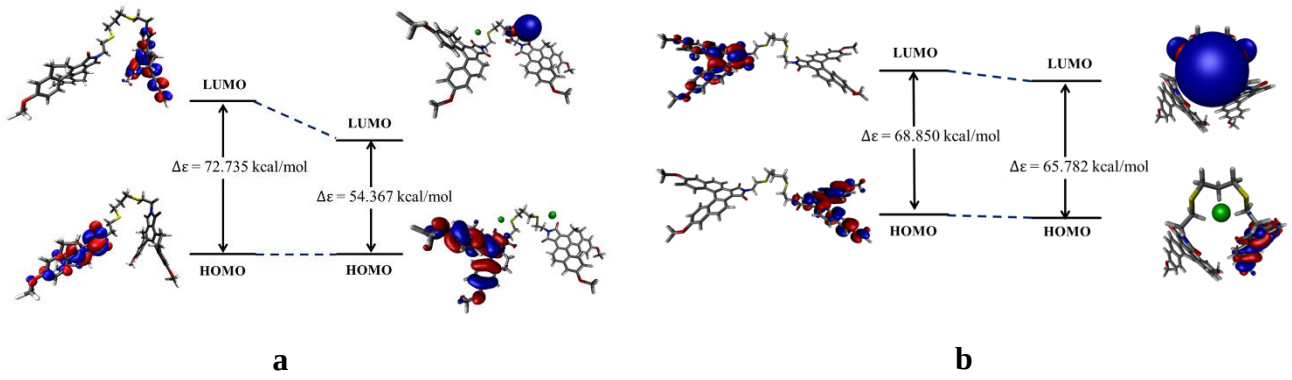

Figure 18 HOMO and LUMO of (a) the **H1** and **H1**:Hg^{2+} and (b) **H1A** and **H1A**:Hg^{2+}

3.7 Application in real samples

Because **H1** exhibited a higher sensitivity for Hg^{2+} detection than **H1A, H1** was chosen for detection of Hg^{2+} in drinking water, river water and digested tuna fillet. Sensor **H1** exhibited a high fluorescence quantum yield, and thus, the fluorescence change when **H1** detected Hg^{2+} was easily noticed by the naked eye under UV light. The fluorescence signals of the **H1** solution with various concentrations of Hg^{2+} in real samples were investigated under UV radiation. As illustrated in Figure 19, similar results of Hg^{2+} detection in real samples using **H1** were obtained. Adding sample solution spiked with Hg^{2+} into the **H1** solution led to a significant decrease in the fluorescence signal. These results indicated that **H1** could be employed as a Hg^{2+} marker in real samples such as drinking water, river water and digested tuna fillet.

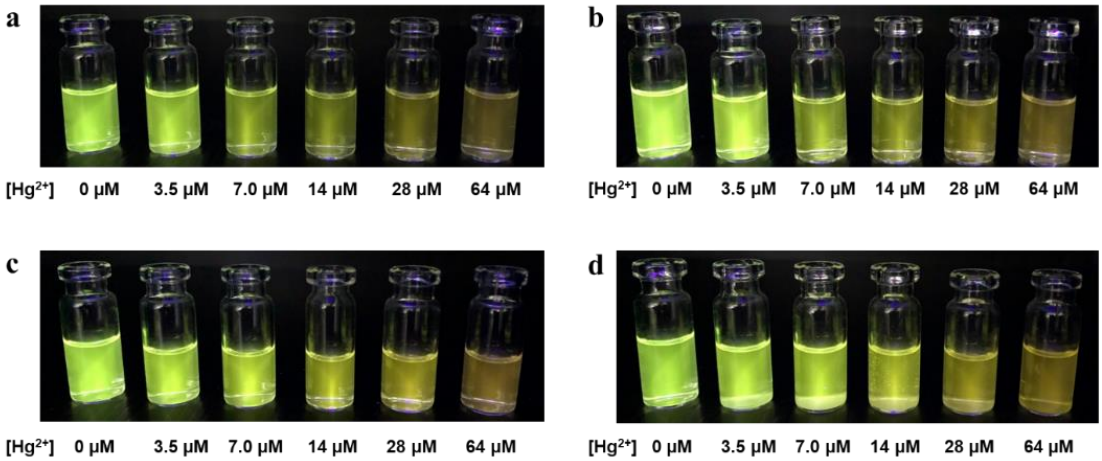

Figure 19 The fluorescence signal of **H1** with the spiking by different concentrations of Hg^{2+} in real samples: (a) drinking water 1; (b) drinking water 2; (c) river water and (d) digested tuna fillet

4. CONCLUSION

Two new fluorescence sensors (**H1** and **H1A**) based on new types of [5]helicene fluorophores connected to 2-(3-(2-aminoethylsulfanyl)propylsulfanyl)ethanamine were successfully synthesized for the detection of Hg^{2+} ions. **H1** and **H1A** illustrated high sensitivity and

selectivity ON-OFF fluorescence quenching when coordinated with Hg^{2+}. **H1** and **H1A** offered very large Stokes shifts of 150 and 198 nm, respectively, which were beneficial for removing analytical error. The sensors provided good Hg^{2+}-selectivity in the presence of high concentrations of foreign ions, in particular, potential competitors such as Cu^{2+}, Ag^{+} and Pb^{2+} as well as Li^{+}, Na^{+}, K^{+}, Ca^{2+}, Fe^{2+}, Cd^{2+}, Zn^{2+}, Mg^{2+}, Ba^{2+}, and Co^{2+}. Moreover, after utilization, **H1** and **H1A** could be reversibly recovered by adding **en**, which made the sensors economical for use in commercial applications. In addition, due to the higher quantum efficiency and lower detection limit of **H1** compared to those of **H1A**, the utilization of **H1** in real samples was investigated. It was found that **H1** demonstrated potential as a Hg^{2+} marker in drinking water, river water and digested tuna fillet.

ACKNOWLEDGEMENT

N. Wanichacheva thanks Grant RSA 6080058 from the Thailand Research Fund and Faculty of Science, Silpakorn University, Thailand. A. Petdum also thanks Thailand Graduate Institute of Science and Technology (TGIST, Grant TG-33-16-59-012D) from National Science and Technology Development Agency (NSTDA), Thailand.

REFERENCES

Bjerrum, J. (1950). On the tendency of the metal ions toward complex formation. *Chemical Reviews*, 46(2), 381-401.

Buckland, D., Bhosale, S. V., and Langford, S. J. (2011). A chemodosimer based on a core-substituted naphthalene diimide for fluoride ion detection. *Tetrahedron Letter*, 52(16), 1990-1992.

Cheng, X., Li, S., Zhong, A., Qin, J., and Li, Z. (2011). New fluorescent probes for mercury(II) with simple structure. *Sensors and Actuators B: Chemical*, 157(1), 57-63.

Dalapati, S., Paul, B. K., Jana, S., and Guchhait, N. (2011). Highly selective and sensitive fluorescence reporter for toxic Hg(II) ion by a synthetic symmetrical azine derivative. *Sensors and Actuators B*, 157(2), 615-620.

Erdemir, S., Malkondu, S., Kocyigit, O., and Alici, O. (2013). A novel colorimetric and fluorescent sensor based on calix[4]arene possessing triphenylamine units. *Spectrochimica Acta Part A: Molecular and Biomolecular Spectroscopy*, 114, 190-196.

Frisch, M. J. et al. (2016). GAUSSIAN 09 (Revision E.01), Gaussian, Inc., Wallingford.

Goswami, S., Manna, A., Paul, S., Das, A. K., Nandi, P. K., Maity, A. K., and Saha, P. (2014). A turn on ESIPT probe for rapid and ratiometric fluorogenic detection of homocysteine and cysteine in water with live cell-imaging. *Tetrahedron Letters*, 55(2), 490-494.

Gu, B., Huang, L., Mi, N., Yin, P., Zhang, Y., Tu, X., Luo, X., Luo, S., and Yao, S. (2015). An ESIPT-based fluorescent probe for highly selective and ratiometric detection of mercury(II) in solution and in cells. *Analyst*, 140(8), 2778-2784.

Gutknecht, J. (1981). Inorganic mercury (Hg^{2+}) transport through lipid bilayer membranes. *The Journal of Membrane Biology*, 61(1), 61-66.

Harada, M. (1995). Minamata disease: methylmercury poisoning in Japan caused by environmental pollution. *Critical Reviews in Toxicology*, 25(1), 1-24.

Hardy, S., and Jones, P. (1997). Capillary electrophoresis determination of methylmercury in fish and crab meat after extraction as the dithizone sulphonate complex. *Journal of Chromatography A*, 791(1-2), 333-338.

Harris, H. H., Pickering, I. J., and George, G. N. (2003). The chemical form of mercury in fish. *Science*, 301(5637), 1203.

Humphrey, W., Dalke, A., and Schulten, K. (1996). VMD: Visual molecular dynamics. *Journal of Molecular Graphics*, 14(1), 33-38.

Kim, S. H., Kim, J. S., Park, S. M., and Chang, S. K. (2006). Hg^{2+}-selective OFF-ON and Cu^{2+}-selective ON-OFF type fluoroionophore based upon cyclam. *Organic Letters*, 8(3), 371-374.

Kim, S. H., Song, K. C., Ahn, S., Kang, Y. S., and Chang, S. K. (2006). Hg^{2+}-selective fluoroionophoric behavior of pyrene appended diazatetrathia-crown ether. *Tetrahedron Letter*, 47(4), 497-500.

Kraithong, S., Damrongsak, P., Suwatpipat, K., Sirirak, J., Swanglap, P., and Wanichacheva, N. (2016). Highly Hg^{2+}-sensitive and selective fluorescent sensors in aqueous solution and sensors-encapsulated polymeric membrane. *RSC Advances*, 6(13), 10401-10411.

Lee, Y. H., Lee, M. H., Zhang, J. F., and Kim, J. S. (2010). Pyrene excimer-based calix[4]arene FRET chemosensor for mercury (II). *Journal of Organic Chemistry*, 75(21), 7159-7165.

Li, M., Lu, H. Y., Liu, R. L., Chen, J. D., and Chen, C. F. (2012). Turn-on fluorescent sensor for selective detection of Zn^{2+}, Cd^{2+}, and Hg^{2+} in water. *The Journal of Organic Chemistry*, 77(7), 3670-3673.

Miao, F., Zhan, J., Zou, Z., Tian, D., and Li, H. (2012). A new Hg^{2+} fluorescent sensors based on 1,3-alternate thiacalix[4]arene (L) and the complex of [L+Hg^{2+}] as turn-on sensor for cysteine. *Tetrahedron*, 68(10), 2409-2413.

Moon, S. Y., Cha, N. R., Kim, Y. H., and Chang, S. K. (2004). New Hg^{2+}-selective chemo and fluoroionphore based upon 8-hydroxyquinoline. *Journal of Organic Chemistry*, 69(1), 181-183.

Ooyama, Y., Matsugasako, A., Nagano, T., Oka, K., Kushimoto, K., Komaguchi, K., Imae, I., and Harima, Y. (2011). Fluorescence PET (photo-induced electron transfer) sensor for water based on anthracene-amino acid. *Journal of Photochemistry and Photobiology A: Chemistry*, 222(1), 52-55.

Park, S. M., Kim, M. H., Choe, J. I. No, K. T., and Chang, S. K. (2007). Cyclams bearing diametrically disubstitutedpyrenes as Cu^{2+}- and Hg^{2+}-selective fluoroionophores. *Journal of Organic Chemistry*, 72(9), 3550-3553.

Renzoni, A., Zino, F., and Franchi, E. (1998). Mercury levels along the food chain and risk for exposed populations. *Environmental Research*, 77(2), 68-72.

Sahasithiwat, S., Mophuang, T., Menbangpung, L., Kamtonwong, S., and Sooksimuang, T. (2010). *3,12*-Dimethoxy-*7,8*-dicyano-[5]helicene as a novel emissive material for organic light-emitting diode. *Synthetic Metals*, 160(11-12), 1148-1152.

Shellaiah, M., Rajan, Y. C., Balu, P., and Murugan, A. (2015). A pyrene based Schiff base probe for selective fluorescence turn-on detection of Hg^{2+} ions with live cell application. *New Journal of Chemistry*, 39(4), 2523-2531.

Song, K. C., Kim, M. H., Kim, H. J., and Chan, S. K. (1996). Hg^{2+}- and Cu^{2+}-selective fluoroionophoric behaviors of a dioxocyclam derivative bearing anthrylacetamide moieties. *Tetrahedron Letter*, 48(42), 7464-7468.

Sooksimuang, T., and Mandal, B. K. (2003). [5]helicene-fused phthalocyanine derivatives. New members of the phthalocyanine family. *The Journal of Organic Chemistry*, 68(2), 652-655.

Sooksimuang, T., Kamtonwong, S., Parnchan, W., Kangkaew, L., and Sahasithiwat, S. (2014). Crystal structure of 3,13-dimethoxy-5,6,10,11-tetrahydrofuro[3,4-i][5]helicene-7,9-dione. *Acta Crystallographica Section E: Crystallographic Communications*, 70(Pt 11), 418-420.

Shortreed, M., Kopelman, R., Kuhn, M., and Hoyland, B. (1996). Fluorescent fiber-optic calcium sensor for physiological measurements. *Analytical Chemistry*, 68(8), 1414-1418.

Suresh, M., Mandal, A. K., Saha, S., Suresh, E., Mandoli, A., Liddo, R. D., Parnigotto, P. P., and Das, A. (2010). Azine-based receptor for recognition of Hg^{2+} ion: crystallographic evidence and imaging application in live cells. *Organic Letters*, 12(23), 5406-5409.

Tchounwou, P. B., Ayensu, W. K., Ninashvili, N., and Sutton, D. (2003). Environmental exposure to mercury and its toxicopathologic implications for public health. *Environmental Toxicology*, 18(3), 149-175.

Thivierge, C., Han, J., Jenkins, R. M., and Burgess, K. (2011). Fluorescent proton sensors based on energy transfer. *Journal of Organic Chemistry*, 76(13), 5219-5228.

Tian, M. H., Ai, Z. J., Ming, D., Yu, D. M., Yu, P., and Ya, W. W. (2010). A simply and highly selective "turn-on" type fluorescent chemosensor for Hg^{2+} based on chiral BINOL-Schiff's base ligand. *Journal of Luminescence*, 130(5), 888-892.

Wanichacheva, N., Siriprumpoonthum, M., Kamkaew, A., and Grudpan, K. (2009). Dual optical detection of a novel selective mercury sensor based on 7-nitrobenzo-2-oxa-1,3-diazolyl subunits. *Tetrahedron Letters*, 50(16), 1783-1786.

Wanichacheva, N., Prapawattanapol, N., Lee, V. S., Grudpan, K., and Petsom, A. (2013). Hg^{2+}-induced self-assembly of a naphthalimide derivative by selective ''turn-on'' monomer/ excimer emissions. *Journal of Luminescence*, 134(6), 686-690.